Phase stability under irradiation in alloys with a positive heat of mixing: Effective thermodynamics description

Raúl A. Enrique and Pascal Bellon
Department of Materials Science and Engineering, and Frederick Seitz Materials Research Laboratory, University of Illinois at Urbana-Champaign, Urbana, Illinois 61801
(Received 4 June 1999)

The alteration of phase stability due to the continuous production of forced atomic displacements, as is the case under irradiation, is studied. A simple kinetic model of a binary alloy exhibiting phase separation is investigated, and two limiting cases are considered: nearest-neighbor ballistic exchanges and arbitrary-length ballistic exchanges. The model is simultaneously studied by direct kinetic Monte Carlo simulations, and by theoretical approaches based in the description of the steady state by effective thermodynamics. Two theoretical frameworks are considered: a microscopic description based in effective interactions, and a macroscopic description based in effective free energies constructed over a modified Cahn-Hilliard equation. Developments of these models are proposed to allow for quantitative predictions. For nearest-neighbor ballistic exchanges, the steady-state phase diagram is evaluated for each of the approaches and the results are directly compared. In the case of arbitrary-length ballistic exchanges, the appearance of labyrinthine mesoscopic structures at steady state is rationalized in terms of the competition between short-range attractive and long-range repulsive effective interactions. The favorable comparison between the theoretical results and the direct Kinetic Monte Carlo simulations shows that the long-term behavior of this inherently far-from-equilibrium system can be described in terms of effective thermodynamic potentials. [S0163-1829(99)05146-2]

I. INTRODUCTION

In several types of applications, materials are continuously maintained away from thermodynamical equilibrium by an external driving force. As examples, we can cite materials under continuous plastic deformation, such as cyclic fatigue or ball milling, and materials under irradiation, such as nuclear reactor core components or compounds produced by ion implantation. The term *driven alloys* has been introduced to refer to this class of systems.[1] Under the forcing condition, the material can reach a steady-state configuration, the properties of which will, in general, be different from the equilibrium properties. In particular, irradiation can affect phase stability in alloys in many different, and seemingly contradictory, ways. For example, while for certain experimental conditions irradiation-induced solute precipitation can take place, in some other conditions enhanced solubility is observed.[2]

For equilibrium systems, thermodynamics and statistical mechanics provide us with a framework to describe the steady state of any system. Driven alloys are, however, systems far from equilibrium, for which thermodynamical concepts cannot be directly applied. The temporal evolution of the driven alloy is described by a non-Hamiltonian (dissipative) dynamical system, so the steady-state probability distribution cannot be written using the equilibrium Gibbs distribution. In fact, no general method exists to find the steady-state probability distribution. Several authors have proposed the construction of *effective* thermodynamical potentials to describe the steady-state properties of the driven alloy. Contrary to equilibrium potentials, these effective potentials depend explicitly on the forcing parameters, since additional intensive variables, related to the strength and particular characteristics of the driving force, must be introduced to specify the steady state.

For a solid under irradiation, the atomic rearrangements produced by a colliding particle have been extensively investigated by molecular dynamics simulations (see Ref. 3 for a recent review). For metals, the magnitude of the atomic displacements produced in the matrix vary according to the energy transferred by the impinging particle, E_p. Above a threshold energy, a sequence of collisions, or ballistic displacements, is originated with the creation of a primary knock-on atom, which is any target struck by the irradiation particle. Lighter particles, such as high-energy electrons, can produce a localized replacement collision sequence (RCS), in which a row of atoms is displaced, with the creation of a vacancy in the first position and an interstitial at the end. On the other hand, neutrons and more massive particles can transfer more energy, generating a collision cascade. Localized regions of the lattice become highly disturbed, and a large amount of mixing takes place. In alloys with positive heat of mixing, for not too energetic cascades, e.g., $E_p \leqslant 1$ keV in Cu (Ref. 4), this atomic mixing appears to be *ballistic*, in the sense that it is not affected by the chemical interactions between atoms. The situation changes for more energetic cascades, as it is the case for $E_p \approx 5$ keV in Co-Cu and Cu-Ni alloys, where it has been observed that an increase in the positive heat of mixing results in a decrease of the atomic mixing.[5] This indicates that the mixing is no longer purely ballistic. In the present work, we restrict ourselves to the case of purely ballistic mixing, as is produced by RCS's or by not too energetic cascades.

A rich gamut of physical situations arise when irradiation-induced mixing acts in opposition to the thermodynamically driven kinetics. Binary systems exhibiting either ordering or

phase separation can be led to different steady-state configurations under the continuous external forcing. The effect of continuous irradiation upon systems with order-disorder transformations has been investigated by numerical simulations and mean-field calculations,[6] where not only extensive solubility has been observed, but also a change of the nature of the $A2$-$B2$ ordering transition from second to first order, which has been later confirmed experimentally.[7] For an alloy exhibiting phase separation, on the other hand, only limited cases have been simulated,[8] and an analysis of the steady state has only been performed in the mean-field approximation.[9,10] Experimental studies of irradiation effects in these types of alloys have been performed extensively.[2] In particular, with 1.0 MeV Kr irradiation, in Ag-Cu samples, Wei and Averback[11] have been able to obtain a solubility enhancement at moderate temperatures, and full solubility at low temperatures, which can be described as a reentrant steady-state miscibility gap.

To explain this type of irradiation-induced mixing experiment, Martin[9] proposed a macroscopic, continuum-based model. In this description, it is assumed that ballistic displacements produce a local mixing of the atoms, and can effectively be described as a diffusion process. Using the Cahn-Hilliard equations, Martin shows that after the addition of the extra diffusion term, an effective free-energy functional can be defined, which is minimum at steady state. For their experimental situation in Ag-Cu, Wei and Averback[11] perform a numerical study based on Martin's formulation to explain qualitatively their results. A similar continuum treatment can be performed for a model of arbitrary-length ballistic exchanges, where at a certain frequency the position of two atoms is interchanged regardless of their separation. It has been observed that an immiscible binary alloy under this type of irradiation develops a steady-state labyrinthine microstructure. An effective free energy can be also defined in this case, which contains an extra term describing an electrostaticlike repulsion between atoms of the same type.[12] The same microstructure can be observed if the alloy undergoes, instead, a nonequilibrium $A \rightleftharpoons B$ chemical reaction.[13]

A different picture of the problem can be constructed starting from an atomistic description. An Ising-type model of competing dynamics, where thermal diffusion and irradiation-induced ballistic exchanges act against each other to drive the system into different directions, has been proposed.[1] At the same time, it allows us to carry out simulations in a statistically meaningful amount of material. Kinetic Monte Carlo (KMC) simulations are required for the system to follow a temporal trajectory, where the meaning of an external irradiation frequency can be maintained. A residence-time algorithm serves to this purpose. This Ising-type model shares the same formal structure with the Ising model in an external field (two-temperatures system or competing dynamics system), that has received attention from the statistical mechanics community.[14–16] Both for the driven alloy and the Ising equivalent, only solutions for low-dimensionality systems or in the mean-field approximation have been found.

The Ising-type description of the system can immediately be put into the form of a master equation for the evolution of the probability of each state of the system. The steady-state probability distribution is the homogeneous solution of the master equation. By considering the general symmetry properties, Vaks and Kamyshenko[10] have shown that the steady-state probability distribution can be rewritten as a Gibbs distribution if one is to define an effective Hamiltonian in terms of pair, triplets, etc., effective interactions. In this way, the problem is reduced to the evaluation of these effective energies. Although it may seem that the existence of an effective Hamiltonian contradicts the statement that no general solution of the problem exists, it must be borne in mind that the effective Hamiltonian will in general be a function of both the temperature and the forcing parameters.[10,15,16] In this work we propose a method to numerically evaluate these effective interactions, from which an analysis of the steady state is carried out by standard equilibrium calculations.

In this paper we study phase stability in a binary alloy with a positive heat of mixing, which continuously undergoes ballistic atomic exchanges due to irradiation. Our focus is in the long-term, steady-state response of such alloy. By performing direct numerical simulations, and comparing the result of these to the predictions of the theoretical models, our purpose is to test the validity range of these approaches at the level of approximation required to perform numerical predictions. Regarding the range of the ballistic exchanges, two limiting models are considered: nearest neighbors and arbitrary-length atomic jumps. Each model case leads to a different type of microstructure. Nearest-neighbor ballistic exchanges represent the mixing produced by a very short RCS, and they induce an enhancement of the solubility in each phase, leading to a closure of the miscibility gap at low temperatures. Arbitrary-length ballistic exchanges, although not corresponding to any specific physical irradiation condition, deserve some attention since they provide useful insight into understanding of the nature of effective interactions in driven alloys. This type of exchange leads to the formation of labyrinthine mesoscopic structures at steady state. In the models, for the sake of simplicity, the concentration of point defects is assumed to have reached a steady value, and the contribution of interstitials, as well as defect sinks and clusters, is neglected. Under these assumptions, the proposed model excludes phenomena related to macroscopic solute migration, such as irradiation-induced heterogeneous precipitation.[2]

The structure of this paper is as follows. We first introduce the microscopic and macroscopic models, and the KMC simulation method. Then we focus on nearest-neighbor ballistic exchanges, performing a direct evaluation of the dynamical phase diagram. The dynamical phase diagram is quantitatively compared to the one derived from Vaks and Kamyshenko's approach, where we devise a method to evaluate numerically the effective interactions, and to the one derived from Martin's model, where we perform quantitative predictions by introducing a mean-field modeling of the chemical diffusion coefficient. We then touch upon the problem of arbitrary-length ballistic exchanges, where labyrinthine mesoscopic structures are observed. By calculating effective interactions, we test the appearance of long-range repulsive effective interactions, which have been used to explain the stabilization of mesoscopic structures.

II. MICROSCOPIC MODEL

The microscopic description is based in an Ising-type model, suited for kinetic Monte Carlo simulations. We con-

sider a binary (AB) alloy on a rigid fcc lattice. Two separate dynamics compete to drive the system into different configurations. On one hand, we have vacancy assisted thermal exchanges that drive the system to thermodynamical equilibrium, i.e., phase separation. On the other hand, we have irradiation-induced ballistic exchanges producing random interchanges of atomic positions. A more detailed presentation of the model can be found in Ref. 17.

The probabilistic evolution of the system is governed by a master equation that describes the transition probability between states of the system:

$$\frac{dP(\alpha)}{dt}=\sum_{\beta} W_{\beta\to\alpha}P(\beta)-W_{\alpha\to\beta}P(\alpha). \tag{1}$$

These transition probabilities are the sum of thermal and ballistic components, $W_{\alpha\to\beta}=W^{\rm th}_{\alpha\to\beta}+W^{\rm ball}_{\alpha\to\beta}$. Each component can be written:

$$W^{\rm th}_{\alpha\to\beta}=\delta^{\rm th}_{\alpha\to\beta}\omega_0 e^{-\beta(E^s_{\alpha\to\beta}-E^{\alpha})}, \tag{2}$$

$$W^{\rm ball}_{\alpha\to\beta}=\delta^{\rm ball}_{\alpha\to\beta}\Gamma_b\,. \tag{3}$$

Here, $\delta_{\alpha\to\beta}$ takes the value 1 of the states α and β are connected by a transition and 0 otherwise, ω_0 is the attempt frequency for vacancy exchange, $E^s_{\alpha\to\beta}$ the saddle-point energy, E^{α} the energy of the configuration, and Γ_b the frequency for ballistic exchanges. The saddle-point energy is independent of the direction of the transition ($E^s_{\alpha\to\beta}=E^s_{\beta\to\alpha}\equiv E^s_{\alpha\leftrightarrow\beta}$). In this model, the total energy of the configuration is obtained as a sum of bonds linking the atoms. Ghost interactions between the vacancy and the atoms are also included to model both the cohesive energy and the vacancy formation energy. In this fashion, the exponent in Eq. (2) is simply a sum of a constant saddle-point energy plus the energy required to break the bonds linking the vacancy and the exchanging atom to their environment. The constant saddle-point term can be fixed by setting a value for the vacancy migration energy at a given concentration.

Although under each separate dynamics detailed balance is satisfied, when considering the competing dynamics, in the most general case, detailed balance is lost. There are, however, specific models for which detailed balance is preserved even in the presence of the two dynamics. For these models, discussed in the Appendix, the equation of detailed balance also acts as a mean to find the steady-state probability distribution.

A. Kinetic Monte Carlo simulations

A residence-time algorithm is used for the kinetic Monte Carlo simulations (a review of this method can be found in Ref. 1). In this way, the system evolves according to Eq. (1) following a temporal trajectory. This property allows for a meaningful comparison between the frequencies of random and vacancy exchanges at each simulation step.

The simulation domain is a $L\times L\times L$ rhombohedric crystal with periodic boundary conditions. The faces of the rhombohedron are $\{111\}$ planes in the fcc crystal. A single vacancy is placed in the simulation domain. Most of the simulations are carried out for $L=64$. When this is not the case, time is rescaled so as to maintain the value for the vacancy concentration $C_v=1/64^3$. The competition between the frequencies for vacancy and ballistic exchanges determines which transition takes place at each time step.

The purpose of the kinetic Monte Carlo simulations is twofold. First, we use it to study the global behavior of the system. Second, we use it to perform a direct numerical evaluation of the effective interactions in Vaks and Kamyshenko formalism, as it is shown below. The material parameters used in the simulation follows the choice made in Ref. 17, and are the following: $e_{aa}=e_{bb}=-0.7233$ eV, $w_{ab}=2e_{ab}-e_{aa}-e_{bb}=0.0553$ eV, $e_{av}=e_{bv}=-0.255$ eV. The latter parameters are the vacancy *ghost* interactions. The ordering energy was chosen so as to reproduce an estimated critical temperature of $T_c=1573$ K$=0.1355$ eV in the Cu-Co system. The vacancy migrates with an attempt frequency $\omega_0=10^{14}$ s^{-1}, and the migration energy for the pure elements is set at $E^m_v=0.8$ eV, values typical for Cu.

B. Effective interactions description

Vaks and Kamyshenko[10] have studied driven binary alloys using an effective interactions formalism. Starting from the master equation that describes the time evolution of the system, Eq. (1), they point out that the most general expression for the steady-state probability distribution can be rewritten in the form:

$$P\{n_i\}=\exp\left(A+\sum_i \lambda_i n_i-\hat{Q}\right), \tag{4}$$

where A is a normalization factor, n_i represents the occupancy of a lattice site by a B atom, and $\hat{Q}$ plays the role of an *effective* Hamiltonian, which can be expressed as an expansion of pair, triplets, etc, effective interactions (notice that the factor k_BT has been absorbed into the energies):

$$\hat{Q}=\sum_{i<j} a_{ij}n_in_j+\sum_{i<j<k} a_{ijk}n_in_jn_k+\cdots. \tag{5}$$

This reformulation does not, however, introduce any simplification to the problem. Since the coefficients in this effective Hamiltonian are, in general, functions of both the temperature and the forcing parameters, for N particles we simply have a transformation in which 2^N unknown quantities (the probabilities of each state) are mapped into a different set of 2^N unknown quantities (the a's coefficients). Still, there is a value in performing this change of variables: a picture in terms of effective interactions is one upon which we can use all the available tools for equilibrium systems.

Unfortunately, no general method exists to perform the evaluation of the effective interactions, beyond mean-field approximations. In principle, if the steady-state probability distribution for any arbitrary configuration is known, evaluation of the effective interactions can be performed by inverting Eq. (4). In this paper, we propose a strategy to evaluate the effective interactions based on a reduced set of KMC simulations, as we explain in the following.

Given two states i and j, the individual probabilities of each state are written $p_i\propto N_i\exp(-q_i)$ and $p_j\propto N_j\exp(-q_j)$, where q_i represents the value of $\hat{Q}$ for the corresponding configuration and N_i the multiplicity. Keeping in mind that

the proportionality constants for the previous equations are the same, we can write the difference in *effective energy* as

$$q_i = q_j - \ln\left(\frac{p_i N_j}{N_i p_j}\right). \tag{6}$$

In particular, to evaluate the pair effective interaction term (first term in the expression for $\hat{Q}$), we perform a simulation of two single B atoms in a pure A matrix. The residence-time algorithm, on which the KMC simulations are based, makes certain that the physical time the two atoms spend at each separation distance can be measured. This time is proportional to the separation probabilities, and by using Eq. (6), we obtain the pair effective interactions. These calculations are performed below for the system under investigation.

The effect of the vacancy in this description must also be analyzed. Strictly speaking, incorporation of a vacancy transforms the binary system into a ternary system, and an added set of effective interactions must be considered. However, in the limit of a very diluted concentration of vacancies, the description of the system as a binary alloy must hold. In fact, the concentrations of vacancies in our simulations is at all times small. During our modeling, the pair effective energies are measured when the vacancy is away from the neighborhood of the B atoms. In this way, we can assure that only the interactions between the B atoms is measured: It can be shown that the pair effective interactions between the vacancy and a B atom is limited to the first neighboring shell, just by direct solution of the corresponding master equation.

III. MACROSCOPIC MODEL

An heuristic, macroscopic description of phase evolution under irradiation was introduced by Martin.[9] An extension for treating arbitrary-length ballistic exchanges was proposed by Pavlovitch and Dobretsov.[12] In each model, the starting point is Cahn and Hilliard's description of thermal diffusion in a binary mixture. An extra term, associated to ballistic mixing, is added to the governing equations.

For nearest-neighbor ballistic exchanges, irradiation mixing can be described as a diffusion process. In this way, the interdiffusion flux can be written

$$-\Omega \mathbf{J} = M \nabla \frac{\delta F}{\delta c} + \mathcal{D}_b \nabla c,$$

$$-\Omega \mathbf{J} = \tilde{D} \frac{c(1-c)}{k_B T} f'' \nabla c + \mathcal{D}_b \nabla c, \tag{7}$$

where Ω is the volume associated to an individual atom, $\mathbf{J}$ is the interdiffusion flux, M the mobility, c the atomic fraction of component B, $\tilde{D}$ the chemical diffusion coefficient, $\mathcal{D}_b$ the ballistic diffusion coefficient, F the total free energy, and f the free energy per unit volume. Having the gradient of composition in both terms in the latter equation allows us to extract common factors. We can then see that the flux is identical to the one for a system in thermodynamical equilibrium whose free energy ϕ has a second derivative:

$$\phi''(c) = f''(c) + \frac{kT}{c(1-c)} \frac{\mathcal{D}_b}{\tilde{D}}. \tag{8}$$

Martin shows that the quantity ϕ is a Lyapunov function of the system, and proposes that it can be used as an effective free energy for the driven alloy. Assuming a constant chemical diffusion coefficient and using the Bragg-Williams approximation, Martin shows that the system behaves as if it was at equilibrium, but at a higher temperature given by

$$T' = T\left(1 + \frac{\mathcal{D}_b}{\tilde{D}}\right), \tag{9}$$

which is known as the effective-temperature criterion. However, to predict phase stability from Eq. (8), one needs to take into account the full dependence of all the terms upon concentration and perform the required integrations in a self-consistent manner. Evaluation of the phase diagram from a free energy makes use of the tangent rule, which is not a local procedure but a global one. A local error in the evaluation of ϕ can have nonlocal consequences in the phase diagram, and the appearance or stability of new phases can be missed by an approximate integration.

In this paper we go beyond Martin's initial assumptions, and take into account the functional dependence of $\tilde{D}$ by a mean-field-based modeling. This allows us to perform quantitative predictions, from which a confrontation to the results of the direct KMC simulations is made.

Pavlovitch and Dobretsov[12] studied the case of arbitrary-length ballistic exchanges. Rather than a diffusion term, this phenomena is described by an exponential decay of the deviations of the concentration around the average value. The equation governing the time evolution of the concentration is

$$\frac{\partial c}{\partial t} = \nabla\left(M \nabla \frac{\delta F}{\delta c}\right) - \Gamma_b (c - \overline{c}), \tag{10}$$

where Γ_b is the ballistic exchange frequency and $\overline{c}$ the average concentration.

Pavlovitch, following an approach first introduced by Leibler[18] and used by Liu and Goldenfeld[19] on a similar equation, points out that if we consider Green's function for Laplace's equation (which is the solution of the electrostatic potential for a point charge):

$$\nabla \cdot \nabla g(\mathbf{r} - \mathbf{r}') = -\delta(\mathbf{r} - \mathbf{r}'), \tag{11}$$

and write a new quantity F^*, to be interpreted as a new effective energy term:

$$F^* = \frac{1}{2} \int d\mathbf{r} \int d\mathbf{r}' [c(\mathbf{r}) - \overline{c}] g(\mathbf{r} - \mathbf{r}') [c(\mathbf{r}') - \overline{c}]. \tag{12}$$

We can then rewrite the diffusion Eq. (10) as

$$\frac{\partial c}{\partial t} = \nabla\left[M \nabla \frac{\delta F}{\delta c} - \Gamma_b \nabla \frac{\delta F^*}{\delta c}\right]. \tag{13}$$

To analyze the meaning of this extra term, we can assume the mobility M to be a constant. We can then regroup terms and define an effective free energy G, as

$$G = F + \frac{\Gamma_b}{M} F^*. \tag{14}$$

Therefore, we reach the conclusion that the system acts as if the effective free energy has an added part that behaves as an electrostatic repulsion between particles of the same type. Since electrostatic fields decay, in three dimensions, as $1/r$, these interactions are long range. Mesoscopic structures, such as those observed in ferrofluids and Langmuir fluids, can be expected.[20] We show below that long-range repulsive interactions also appear in the microscopic description based in effective interactions.

IV. NEAREST-NEIGHBOR BALLISTIC EXCHANGES

In a binary alloy exhibiting phase separation, a constant frequency of nearest-neighbor ballistic exchanges produces a solubility enhancement. At low enough temperature, it causes solubility in the whole concentration range. Phase segregation still proceeds in a way similar to equilibrium, with the system separating into two macroscopic phases of rich *A* and *B*. At steady state, we can still evaluate a steady-state dynamical phase diagram, describing the phases at a given temperature and ballistic frequency. This dynamical phase diagram is described in a three-parameters space: (c,T,Γ_b). We first consider the (c,T) space, evaluating the dynamical phase diagram for three given values of Γ_b. The results are then compared to the predictions of the microscopic model based in effective interactions, and of the macroscopic model based in effective free energies. At the end, we show the results for the chosen parameters in the (T,Γ_b) space.

A. Dynamical phase diagram

Due to the lack of a grand canonical formalism for the driven alloy, only simulations that conserve the global composition can be performed. The miscibility gap is built by letting the system evolve into steady-state separate phases and measuring the local concentration in each phase.

The lower and upper limits of the miscibility gap (which we shall call the lower and upper critical temperatures) are determined using the fourth-order cumulant method,[21] yielding these critical temperatures with excellent accuracy ($\approx 0.3\%$). The finite-size analysis of the fourth-order cumulant is made with statistical analysis of small boxes of sides $L_b = 4,6,8,10,12$ contained in the simulation domain. This analysis shows to be unaffected by the constraint of conserved global concentration.

Figure 1 shows a series of dynamical phase diagrams at the ballistic frequencies $\Gamma_b = 10^2,\ 10^5,\ 5\times 10^5\ \mathrm{s}^{-1}$.

B. Effective pair interactions

The dynamical phase diagram can also be evaluated from a different perspective using Vaks and Kamyshenko formalism. Once the effective interactions are obtained, any available technique for evaluation of equilibrium phase diagrams, such as grand canonical calculations, can be used. In this paper we consider an approximate effective Hamiltonian $\hat{Q}$ by neglecting terms beyond pair effective interactions.

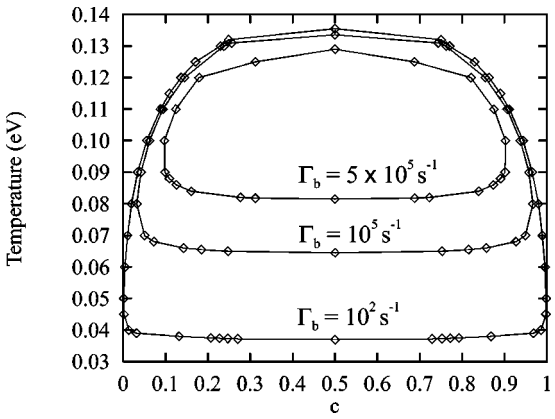

FIG. 1. Steady-state dynamical phase diagrams at three constant frequencies of nearest-neighbor ballistic exchanges: $\Gamma_b = 10^2,\ 10^5$, and $5\times 10^5\ \mathrm{s}^{-1}$.

As explained before, to evaluate the effective pair interactions we measure the time two isolated *B* atoms spent at each separation distance in a rich *A* matrix. The accuracy by which relative probabilities can be measured in this way decays with the inverse of the root of the number of iterations. Due to this slow convergence, long simulations are required. To reduce the computation time, we perform these simulations in a smaller box, of size $L = 12$. Since we still have only one vacancy, and the temporal evolution of the system is proportional to the vacancy concentration, we rescale the time accordingly to maintain the reference value $C_v = 1/64^3$. We keep track of the time spent by the two atoms at the first tenth separation distances, and since only differences of effective energies can be measured, as stated by Eq. (6), we use as reference the longest separation distance.

Proceeding in this way we obtain a series of effective energies as a function of temperature, as shown in Fig. 2 for $\Gamma_b = 10^2\ \mathrm{s}^{-1}$. As we can observe in the figure, effective interactions are temperature dependent. At high temperatures, where thermal diffusion is dominant, the effective interac-

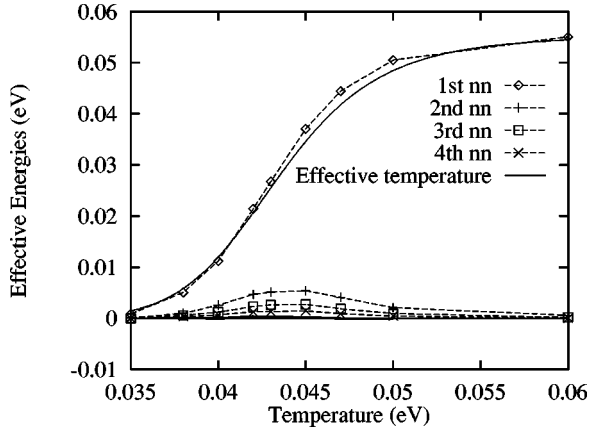

FIG. 2. Effective pair interaction energies for several separation distances as a function of the temperature, for a constant $\Gamma_b = 10^2\ \mathrm{s}^{-1}$. Nonzero effective interactions are observed up to the fourth nearest-neighbor (4th nn) shell. The remaining pair effective interactions are also plotted as lines, and have a negligible value. The solid line corresponds to the prediction of the first nearest-neighbor effective ordering energy using Martin's effective-temperature criterion.

tions simply match the physical ones. At low temperatures, on the other hand, where thermal diffusion is slow and ballistic exchanges dominate, the system is led to a random solid solution, what is reflected by a negligible value of the effective ordering energies. At intermediate temperatures we have a competition between the two regimes, and what is interesting, we observe that the effective interactions extend beyond the range of the physical ones, i.e., beyond the first shell. In fact, nonzero effective ordering energies are observed up to the fourth nearest-neighbor shell. As it is shown in the Appendix, this is a reflection of the lack of detailed balance in this driven alloy.

From the set of effective energies for the three values of Γ_b, we evaluate the corresponding equilibrium phase diagram, using standard grand canonical equilibrium Monte Carlo simulations. The fourth-order cumulant method is used to obtain the critical temperatures. This series of phase diagrams compare surprisingly well with the original phase diagram, as we can see in Fig. 3, even though we restricted ourselves to pair effective interactions.

C. Effective free energy

Here we obtain the dynamical phase diagram using Martin's effective free-energy formalism. Evaluation of the effective free energy requires knowledge of functional form of the equilibrium free energy, $f(c,T)$, and the chemical diffusion coefficient, $\tilde{D}(c,T)$. In this work, as in Martin's original paper,[9] we use for $f(c,T)$ the expression obtained in the Bragg-Williams approximation. We, however, introduce a mean-field-based modeling to obtain the chemical diffusion coefficient, as it is shown in the following.

The chemical diffusion coefficient is written $\tilde{D}=cD_1^*+(1-c)D_2^*$, where D_i^* are the individual tracer diffusion coefficients. These can be expressed as $D_i^*=\frac{1}{12}C_v f_i a_0^2 \Omega_i$, where Ω_i is the exchange frequency and f_i the correlation factor, for an atom of type *i*.

The correlation factor is an important contribution to the diffusion coefficient when trapping occurs: At low temperature and low concentrations, a vacancy exchanging with a solute atom will exchange with it again with a great probability. For f_i, we use the expression recently derived by Nastar *et al.*,[22]

$$f_i=\frac{(2-c_i\lambda)f_0}{2-\lambda(2-c_i-2f_0+2c_i f_0)}, \tag{15}$$

where f_0 is the correlation factor for vacancy mechanism diffusion on a fcc lattice, and the quantity λ is defined as

$$\lambda=1-\exp\{\beta[-zw_{ab}c_a+z(U+w_{ab})/2]\},$$

where z is the coordination number of the lattice and U is the asymmetry parameter, $U=e_{aa}-e_{bb}$.

The frequencies for vacancy-atom exchange are evaluated in a mean-field approximation, assuming that each particle is surrounded by an average environment determined by the local composition. In this way, for an *A* atom neighboring to a vacancy, this *mean-field* energy required to break the bonds is

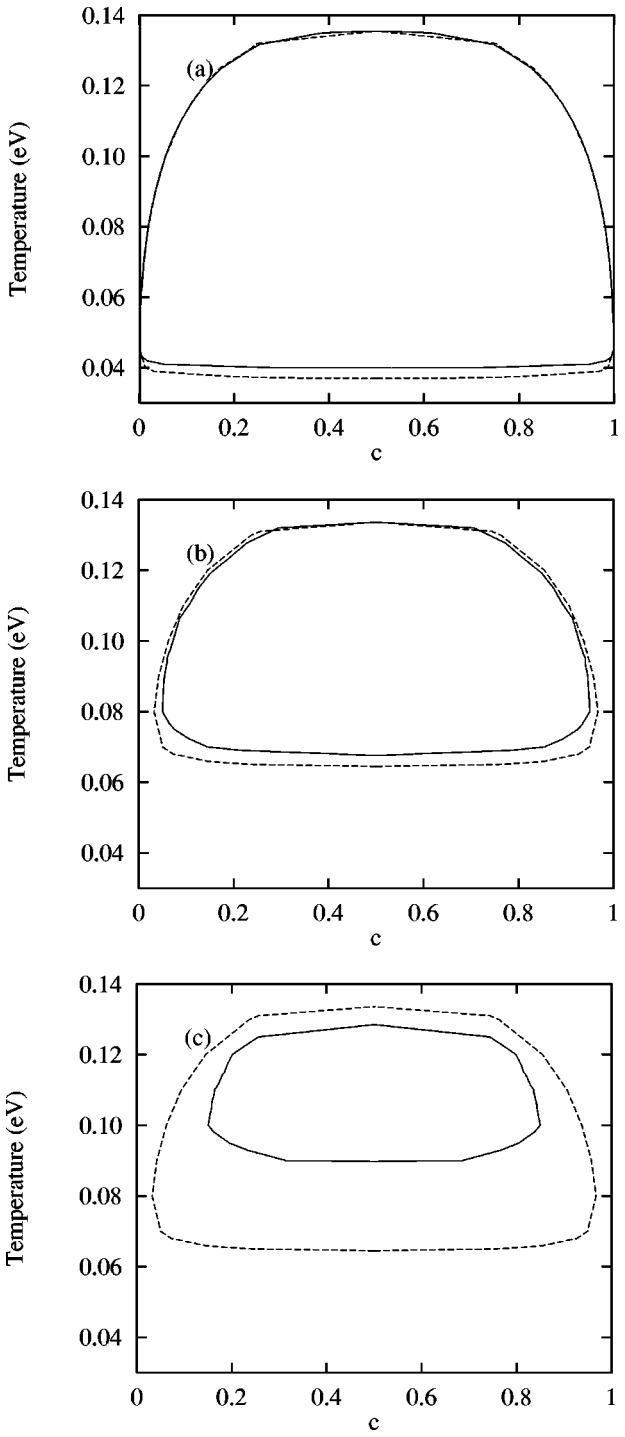

FIG. 3. Dynamical phase diagram computed using effective pair interactions (solid line). The actual dynamical phase diagram is also shown (dashed lines) for comparison. Plotted lines are linear interpolation between computed data points. (a) $\Gamma_b=10^2\ \mathrm{s}^{-1}$. (b) $\Gamma_b=10^5\ \mathrm{s}^{-1}$. (c) $\Gamma_b=5\times10^5\ \mathrm{s}^{-1}$.

$$(E_{\mathrm{mf}}^{\mathrm{BB}})^{(a)}=(z-1)ce_{bv}+(z-1)(1-c)e_{av}+e_{av}+(z-1)ce_{bb}+(z-1)(1-c)e_{ab}. \tag{16}$$

The corresponding exchange frequency is then obtained using Eq. (2).

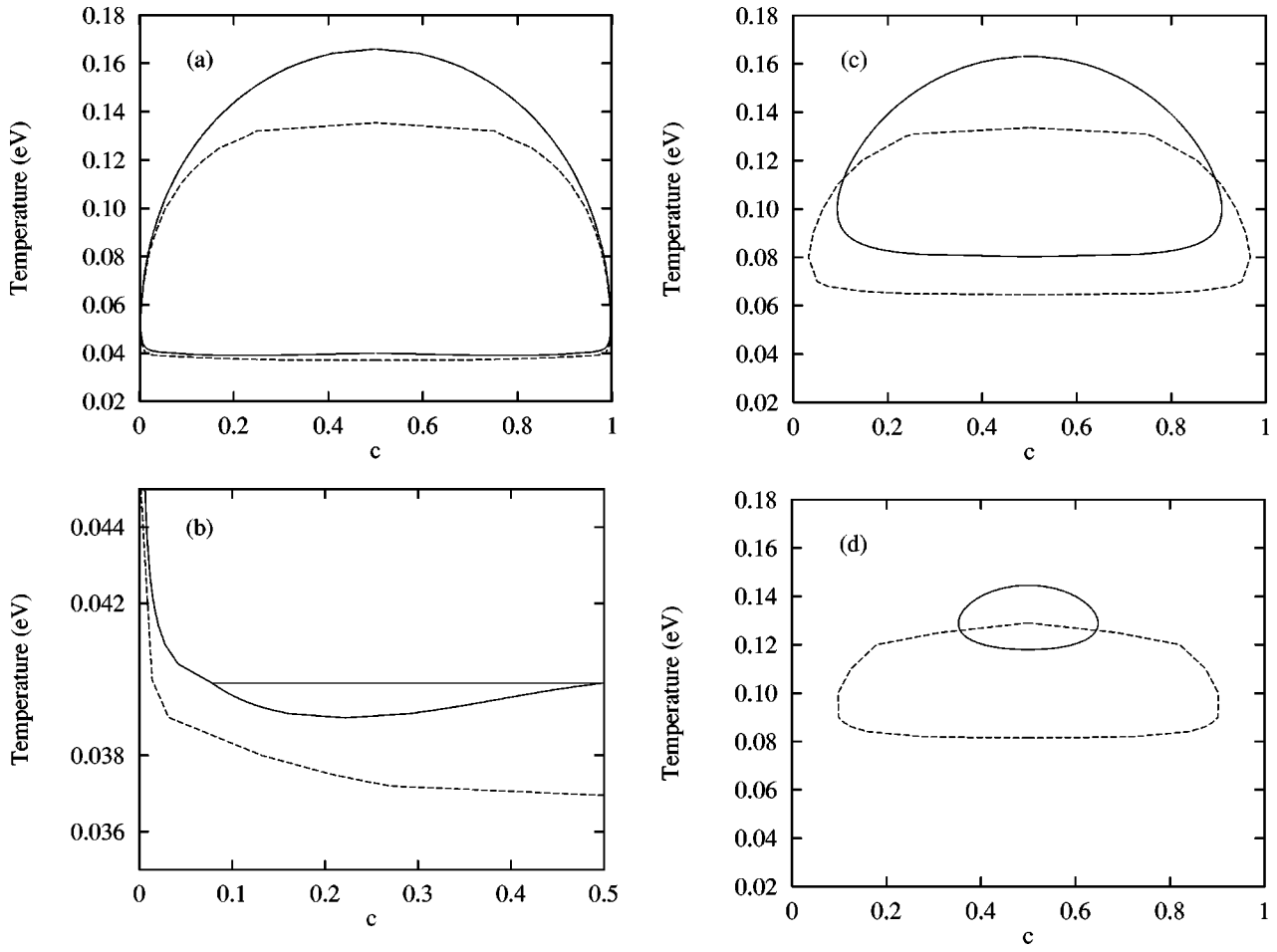

FIG. 4. Phase diagram computed using the effective free energy from Martin's macroscopic model (solid line). The exact dynamical phase diagram (dashed line) is also shown for comparison. (a) $\Gamma_b = 10^2\ \mathrm{s}^{-1}$. (b) Close up at low temperatures showing a three-phase coexistence line. (c) $\Gamma_b = 10^5\ \mathrm{s}^{-1}$. (d) $\Gamma_b = 5\times 10^5\ \mathrm{s}^{-1}$.

From the detailed dependence of f and $\tilde{D}$ with the concentration and temperature, we perform numerically the double integration required in Eq. (8) to evaluate the effective free energy, ϕ. The miscibility gap is constructed making use of the common tangent rule. Since ϕ is only a Lyapunov function,[9] the common tangent rule may not apply strictly, but it should be a reasonable approximation. The resulting phase diagrams are shown in Fig. 4 for the three ballistic frequencies. For comparison, the actual dynamical phase diagram is plotted in dashed lines. At high temperatures, in all the plots, we observe the well-known discrepancies due to the Bragg-Williams approximation. At $\Gamma_b = 10^2\ \mathrm{s}^{-1}$, the macroscopic model reproduces very well the closure of the miscibility gap at low temperatures. The accuracy of the prediction decreases, however, as Γ_b is increased. Quite surprisingly, the macroscopic model presents a feature not observed so far in the simulations: the existence of a three-phase line at low temperatures, what we will refer to as a quasiperitectoid. This feature appears because of the extra term in ϕ, which having its own curvature when plotted as a function of the concentration, causes the existence of two local maxima at low temperatures. These maxima disappear at high temperatures, and the transition point between the two regimes can be found by locating the zero of the fourth derivative of ϕ, and takes the set of numerical values ($k_B T = 0.0752$ eV, $\Gamma_b = 6.5\times 10^4\ \mathrm{s}^{-1}$).

D. Discussion

To summarize the results of this section, Fig. 5 represents a cut of the dynamical phase diagram in the (T,Γ_b) space, at the $c = 0.5$ composition. This plot contains the predictions for the lower and upper critical temperature for all the models considered. This type of cut can be thought of as a (P,T) diagram in an equilibrium system.

Both Fig. 3 and Fig. 5 show that a truncation of the effective Hamiltonian $\hat{Q}$ to pair effective interactions constitutes a very good approximation to the behavior of the system. The differences between the actual phase diagram and this approximation are due to the many-body terms that were dropped out. The next approximation level, the three-body effective interactions, can be evaluated in a similar fashion as the pair terms, by performing a simulation of 3 B atoms sitting in a pure A matrix. This term would be required if we were interested in an alloy with an asymmetrical dynamical phase diagram, which would appear, for example, if $e_{aa} \neq e_{bb}$.[10]

Quite interestingly, the temperature dependence of the first nearest-neighbor ordering energy, as seen in Fig. 2, is very well described by Martin's effective-temperature criterion, Eq. (9), where we have set $\tilde{D} \equiv \tilde{D}(c = 0.5, T)$. The solid line in this figure represents the increase of the effective temperature as an effective reduction of the ordering energy.

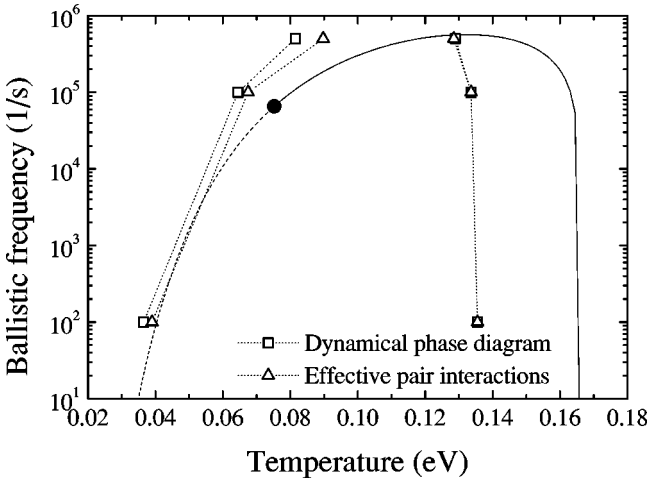

FIG. 5. Dynamical phase diagram in the (T,Γ_b) space, at a concentration $c=0.5$. The line is the prediction of the macroscopic model. The dashed part of this line corresponds to the set of temperatures at which there is a three-phase coexistence line. For the three values of Γ_b investigated, the results for the actual phase diagram are shown as triangles, and the predictions of the effective pair interactions formulation are shown as squares.

Not only is the lower critical temperature well predicted, but also the behavior for the whole temperature range. At higher temperatures, the favorable qualitative comparison remains, although the quantitative comparison fails.

In Fig. 5, the plotted line represents actually the lower and upper limits of the spinodal line in Martin's model. Here, the existence region for the quasiperitectoid is indicated by a dashed line. In the ordinary two-phase region, the lower limit of the spinodal equals the lower critical temperature, and in the quasiperitectoid region, it is a good approximation to it due to the short temperature interval at which the coexistence of three phases appear. The right-hand side of the curve for the macroscopic model shows clearly the limitations of the Bragg-Williams approximation. These results could have been plotted in terms of a reduced temperature, by scaling respect to the critical temperature. However, this scaling would be extraneous to the modeling presented here, which is based in evaluating free energies at given temperatures and concentrations, and does not allow for intermediate expression of the involved parameters in terms of reduced temperatures, due to the functional complexity of the chemical diffusion coefficient. The left-hand side of the curve (the lower critical temperature), shows a very good agreement to the actual dynamical phase diagram, especially at low temperatures.

For the macroscopic description of the system under nearest-neighbor ballistic exchanges, we observe that by considering a concentration dependent chemical diffusion coefficient, irradiation effects are not simply equivalent to a higher effective temperature.[9] Furthermore, this new evaluation of Martin's model suggests that three phases may coexist in dynamical equilibrium at low temperatures. This prediction has not been observed so far in our KMC simulations, where tests were carried out around the lower critical temperature to detect it. Although this feature could be an artifact created by either the mean-field approximation, or the use of a Lyapunov function as a potential for global stability, its existence should not be completely discarded at lower temperatures. A quasiperitectoid structure in the phase diagram is appealing when considering experimental results in other types of driven alloys. In ball milling of Ag-Cu powders, where the continuous mixing produced by the plastic deformation parallels mixing by irradiation, the dynamical coexistence of a 50% composition phase with the two rich solid solutions has been proposed to rationalize x-ray diffraction results.[23]

V. ARBITRARY-LENGTH BALLISTIC EXCHANGES

We now turn our attention to the case of arbitrary-length ballistic exchanges. As it was mentioned in the Introduction, it does not represent strictly a physical situation, although it could be realized in certain experimental conditions. Indeed, during a collision cascade, vacancy and interstitial clusters can be created.[24] Some of these interstitial clusters have a great mobility,[25] in some cases with an apparent activation barrier as low as 0.02 eV,[26] and as a consequence atoms can relocate at much greater speed than by vacancy-assisted thermal diffusion. Arbitrary-length ballistic exchanges represent a limit case for this fast relocation of interstitials created in collision cascades; it is also worthwhile to study because it induces a very different steady-state microstructure, with a labyrinthlike pattern, and suggests that this kind of pattern can be generated by irradiation.

Labyrinthine mesoscopic structures can be observed in the KMC simulations for a range of Γ_b values. If Γ_b is too high, the dominant ballistic exchanges produce a random solid solution. However, at lower values of Γ_b, for instance, for $k_BT=0.03447$ eV, $\Gamma_b<10^2$ s^{-1}, the type of microstructure shown in Fig. 6 can be found. This figure is a (111) cut of the simulation cell at steady state. Although the microstructure fluctuates in time, the width of the rich A and B regions have reached a steady value. This characteristic length increases as Γ_b is decreased, following a power law with a $-1/3$ exponent, in agreement with the analysis performed by Liu and Goldenfeld[19] on a modified Cahn-Hilliard equation similar to Eq. (10), but used for modeling block copolymer melts. The steady-state characteristic length can be made as large as the size of the simulation cell, and we can assume that if larger simulation cells are used (which would require longer simulation times), larger steady-state characteristic lengths could be observed.

By measuring the effective pair energies in the same way it was done for the nearest-neighbor ballistic exchanges problem, we can test the explanation of the origin of the mesoscopic structures, which was based in the existence of a repulsive long-range effective energy. Figure 7(a) shows effective energies for different ballistic frequencies Γ_b, at a constant temperature $k_BT=0.03447$ eV. Figure 7(b) shows the same effective energies, but now plotted as a function of $1/r$, the inverse of the separation distance, for each value of Γ_b. Notice that only energies beyond the first shell are plotted. The straight line appearance of the energies in this plot shows us the consistency between the idea of an effective electrostaticlike repulsion and the measured effective pair interactions.

Labyrinthine mesoscopic structures have also been observed by Glotzer *et al.*,[13] in an Ising model where a Ka-

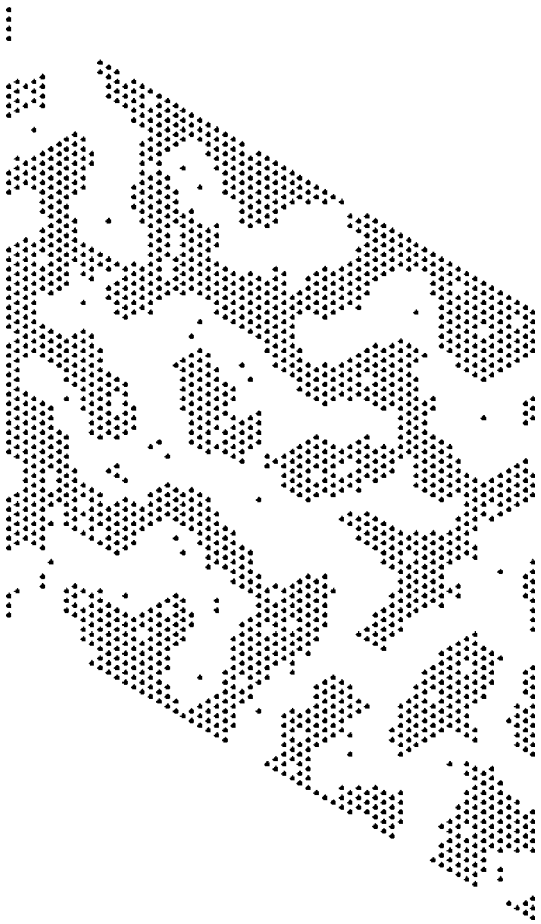

FIG. 6. Steady-state microstructure for arbitrary-length ballistic exchanges. Figure shows a (111) cut of the simulation cell, where A and B atoms are represented as white and dark discs, respectively. $k_BT=0.03447$ eV, $\Gamma_b=10^{-1}$ s^{-1}.

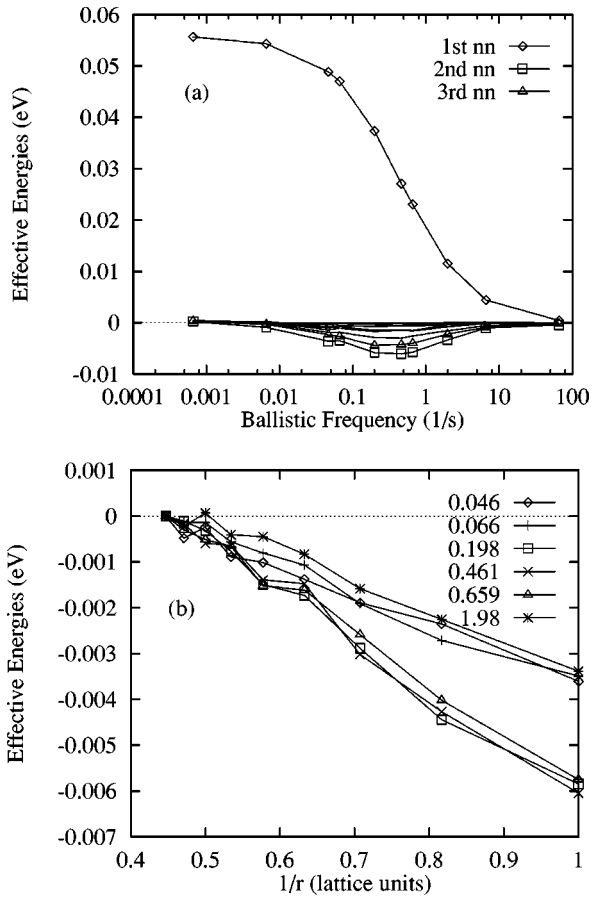

FIG. 7. Effective energies at several ballistic frequencies for arbitrary-length ballistic exchanges at a constant temperature $k_BT=0.03447$ eV. (a) Plotted as a function of the ballistic frequency for each separation distance. The interactions are attractive in the short range, but change sign and are repulsive beyond the first shell. (b) Plotted as a function of the inverse of the separation distance $(1/r)$ for each ballistic frequency, showing the long-range behavior. The lines connecting the points are a visual aid to follow each set of results.

wasaki exchange dynamics competes with a chemical reaction $A \rightleftharpoons B$. The similarity between this chemical reaction and arbitrary-length ballistic exchanges can be immediately drawn, by considering that ''for each A that becomes a B, there is a B that becomes an A.''[13] Indeed, the Cahn-Hilliard-type macroscopic equation describing both systems is the same. Another system sharing the same macroscopic description is a block copolymer melt, where the labyrinthine structures have been studied both experimentally and theoretically.[18,19] In fact, an effective free-energy functional with a long-range electrostaticlike repulsion was first derived by Leibler[18] for these polymer systems.

It is worth noting that mesoscopic structures, in the form of a distribution of $L1_2$ ordered precipitates in coexistence with the fcc solid solution, have been reported in Ni-Al after 100 keV Ni^+ ion irradiation at 550 °C (Ref. 27). Starting from a sample with a distribution of precipitates, an *inverse coarsening* effect is observed under irradiation, with the average precipitate diameter shrinking to a final size. Further experimental work is needed in order to determine whether this microstructure is a result of the kinetic effects studied here, or whether it is induced by a distribution of dislocation loops, as observed, for instance, in Ni_4Mo.[28]

VI. CONCLUSION

The steady-state of a binary alloy with a positive heat of mixing subjected to continuous ballistic atomic exchanges is modeled using several tools: KMC, microscopic effective interactions, and macroscopic effective free energies. Nearest-neighbor ballistic exchanges, simulating short replacement collision sequences (RCS), lead to an enhancement of the solubility in the immiscible system, which in analogy to the equilibrium situation, can be described by a *dynamical* phase diagram with a miscibility gap closing down at low temperatures. In the opposite limit for the atomic displacements, arbitrary-length ballistic exchanges lead to the stabilization of labyrinthine mesoscopic structures.

Kinetic Monte Carlo simulations are performed to evaluate the dynamical phase diagram, and by direct comparison to the predictions of two theoretical approaches (effective

interactions and effective free energies), we show the suitability of these frameworks to approximate the dynamical phase diagrams. Small discrepancies are found, attributable to the approximations made in each case. However, the agreement is encouraging enough to state that these inherently far from equilibrium systems admit a description in terms of effective thermodynamics. In particular, is surprising the accuracy of the predictions based on pair effective interactions, where a huge extrapolation is made: The behavior of the whole system is predicted by simulations of two particles in a lattice.

A microscopic description in terms of effective interactions shows us that although physical interactions are restricted to first nearest neighbors, effective interactions extend beyond the first shell. This change in the nature of the interactions can be a way to understand the change of microstructural features in driven alloys, such as the change of shape of precipitates under irradiation.[8] This change in the nature of the interactions occur in a more dramatic way for arbitrary-length ballistic exchanges, where long-range repulsive effective interactions help to rationalize the stabilization of steady-state mesoscopic structures.

As discussed earlier, nearest-neighbor ballistic exchanges can be viewed as a very short RCS, involving only two atoms. Experiments and computer simulations indicate that the length of these RCS's is rather in the range of 3 to 10 atoms.[3] In our current studies, preliminary results indicate that mesoscopic structures can be observed at steady state with such RCS's, in agreement with results already obtained by Haider.[29] Further work is under progress to understand why the stabilization of mesoscopic structures is so sensitive to the length of the RCS.

ACKNOWLEDGMENTS

Stimulating discussions with G. Martin, M. Nastar, and B. Legrand are gratefully acknowledged. This work was supported by the U.S. Department of Energy Grant No. DEFG02-96ER45439 through the University of Illinois Materials Research Laboratory. The present simulation work has greatly benefited from the MRL Center for Computation.

APPENDIX: DETAILED BALANCE IN THE DRIVEN ALLOY

The idea in this short section is to present a discussion about the connection between the loss of detailed balance and the change in the nature of the effective interactions. In the following, we will show that: (1) Certain models of competing dynamics can obey detailed balance. (2) When detailed balance is obeyed, the range of the effective interactions is restricted by the range of the physical interactions. Rather than perform strict formal proofs, our intention is to sketch the underlying relationship.

Let us start by assuming detailed balance holds in a driven alloy. Without considering any particular dynamics in the phase space of possible configurations, let us assume it is complex enough to be far from one dimensional. It is clear that detailed balance holds when states can be ordered in a line, with transitions occurring only between neighboring states. Now, if we take a close path in the space of configurations, i.e., a sequence of the type

$$\alpha \rightarrow \beta \rightarrow \gamma \rightarrow \cdots \rightarrow \omega \rightarrow \alpha,$$

by multiplying all the equations of detailed balance for the individual transitions we obtain

$$\frac{P(\alpha)}{P(\beta)}\frac{P(\beta)}{P(\gamma)}\cdots\frac{P(\omega)}{P(\alpha)} = \frac{W_{\alpha\rightarrow\beta}}{W_{\beta\rightarrow\alpha}}\frac{W_{\beta\rightarrow\gamma}}{W_{\gamma\rightarrow\beta}}\cdots\frac{W_{\omega\rightarrow\alpha}}{W_{\alpha\rightarrow\omega}} = 1.$$

In terms of the dynamical parameters, this equation can be written

$$\frac{\Gamma_b + W^{\mathrm{th}}_{\alpha\rightarrow\beta}}{\Gamma_b + W^{\mathrm{th}}_{\beta\rightarrow\alpha}}\frac{\Gamma_b + W^{\mathrm{th}}_{\beta\rightarrow\gamma}}{\Gamma_b + W^{\mathrm{th}}_{\gamma\rightarrow\beta}}\cdots\frac{\Gamma_b + W^{\mathrm{th}}_{\omega\rightarrow\alpha}}{\Gamma_b + W^{\mathrm{th}}_{\alpha\rightarrow\omega}} = 1. \quad \text{(A1)}$$

According to our assumption, this equation must hold for all values of Γ_b. But in terms of Γ_b, what we have is the ratio of two polynomials equal to one, each polynomial with a unity leading coefficient. Therefore, the roots of each polynomial must be equal, which simply means that the exponential terms in the jump frequencies for diffusion must coincide. Let us make the assumption that this can only impose a *local* condition upon the transitions in each state or upon the transitions between two states.

These requirements of locality can only be satisfied in two ways. The first possible condition is that

$$W^{\mathrm{th}}_{\alpha\rightarrow\beta} \equiv W^{\mathrm{th}}_{\alpha}, \quad \text{(A2)}$$

where terms for transitions beginning at one state will cancel each other ($W_{\alpha\rightarrow\beta}$ cancels $W_{\alpha\rightarrow\gamma}$, etc.), and is equivalent to a constant saddle-point energy for all transitions. The second possible condition is that

$$W^{\mathrm{th}}_{\alpha\rightarrow\beta} \equiv W^{\mathrm{th}}_{\beta\rightarrow\alpha}, \quad \text{(A3)}$$

where transition terms from two states will cancel each other ($W_{\alpha\rightarrow\beta}$ cancels $W_{\beta\rightarrow\alpha}$, etc.), and means that all the states have the same base energy, with possibly a different saddle-point energy for each transition. The inverse relation is also true: if either of these two restrictions hold, it is straightforward to show that detailed balance is satisfied, simply by inspection.

Let us suppose that we are dealing with one of these systems. Then, for two connected states:

$$\frac{P_\alpha}{P_\beta} = \frac{\Gamma_b + \omega_0 e^{-\beta(E^s_{\alpha\leftrightarrow\beta} - E^\alpha)}}{\Gamma_b + \omega_0 e^{-\beta(E^s_{\alpha\leftrightarrow\beta} - E^\beta)}}, \quad \text{(A4)}$$

which means that if their original energy is the same, their steady-state probabilities must be the same. Hence, by Eq. (4), their effective energies must coincide. From here, the proof that the range of the effective interactions is limited by the range of the physical ones can be performed in a constructive manner, starting from the pair terms and moving onto the many body terms. By considering two *B* atoms in a pure *A* matrix that are, already, far away from their physical influence, we see that the atoms can be separated even further away by a thermal diffusion step. Both states must therefore have the same effective energy, which proves that the effective *pair* interaction cannot have a range longer than the physical *pair* interaction. In the same manner, by adding

another *B* atom and repeating the argument, we can see that the effective *triplet* interaction term must have a range bounded by the physical *triplet* interaction, and so on. As a result, if detailed balance holds, effective energies must share the range of the original physical energies, and long-range effective interactions can only appear when detailed balance is lost. Notice that even if detailed balance is observed, these effective interactions are still a function of both the temperature and the external driving force (expressed by Γ_b in this case).

[1] G. Martin and P. Bellon, Solid State Phys. **50**, 189 (1997).
[2] K.C. Russel, Prog. Mater. Sci. **28**, 229 (1984).
[3] R.S. Averback and T. Diaz de la Rubia, Solid State Phys. **51**, 281 (1998).
[4] H. Gades and H.M. Urbassek, Phys. Rev. B **51**, 14 559 (1995).
[5] K. Nordlund and R.S. Averback, Phys. Rev. B **59**, 20 (1998).
[6] F. Soisson, P. Bellon, and G. Martin, Phys. Rev. B **46**, 11 332 (1992); P. Bellon, *ibid.* **45**, 7517 (1992); F. Haider, P. Bellon, and G. Martin, *ibid.* **42**, 8274 (1990).
[7] F. Soisson, P. Dubuisson, P. Bellon, and G. Martin, in *Solid → Solid Phase Transformations*, Proceedings of the International Conference, Farmington, Pennsylvania, 1994, edited by W. C. Johnson, J. M. Howe, D. E. Laughlin, and W. A. Soffa (TMS, Warrendale, PA, 1994).
[8] P. Bellon, Phys. Rev. Lett. **81**, 4176 (1998).
[9] G. Martin, Phys. Rev. B **30**, 1424 (1984).
[10] V.G. Vaks and V.V. Kamyshenko, Phys. Lett. A **177**, 269 (1993).
[11] L.C. Wei and R.S. Averback, J. Appl. Phys. **81**, 613 (1997).
[12] A. Pavlovitch and V. Yu. Dobretsov, Commissariat à l'Énergie Atomique Report No. CEA-SRMP-97-85, 1997 (unpublished), p. 50.
[13] S.C. Glotzer, E.A. Di Marzio, and M. Muthukumar, Phys. Rev. Lett. **74**, 2034 (1995); S.C. Glotzer and A. Coniglio, Phys. Rev. E **50**, 4241 (1994); S.C. Glotzer, D. Stauffer, and N. Jan, Phys. Rev. Lett. **72**, 4109 (1994).
[14] A. Szolnoki, G. Szabó, and O.G. Mouritsen, Phys. Rev. E **55**, 2255 (1997).
[15] B. Bergersen and Z. Rácz, Phys. Rev. Lett. **67**, 3047 (1991).
[16] P.L. Garrido and J. Marro, Phys. Rev. Lett. **62**, 1929 (1989).
[17] P. Bellon and R.S. Averback, Phys. Rev. Lett. **74**, 1819 (1995).
[18] L. Leibler, Macromolecules **13**, 1602 (1980).
[19] F. Liu and N. Goldenfeld, Phys. Rev. A **39**, 4805 (1989).
[20] M. Seul and V.S. Chen, Phys. Rev. Lett. **70**, 1658 (1992).
[21] K. Binder and D. W. Heermann, *Monte Carlo Simulations in Statistical Physics* (Springer, Heidelberg, 1997), p. 44.
[22] M. Nastar, V. Yu. Dobretsov, and G. Martin, Philos. Mag. A (to be published).
[23] T. Klassen, U. Herr, and R.S. Averback, Acta Mater. **7**, 2921 (1997).
[24] K. Nordlund, M. Ghaly, R.S. Averback, M. Caturla, T. Diaz de la Rubia, and J. Tarus, Phys. Rev. B **57**, 7556 (1998).
[25] B.D. Wirth, G.R. Odette, D. Maroudas, and G.E. Lucas, J. Nucl. Mater. **244**, 185 (1997).
[26] Yu.N. Osetsky, D.J. Bacon, and A. Serra, Philos. Mag. Lett. **79**, 273 (1999).
[27] R.S. Nelson, J.A. Hudson, and D.J. Mazey, J. Nucl. Mater. **44**, 318 (1972).
[28] P. Bellon, P.R. Okamoto, and G. Schumacher, J. Nucl. Mater. **205**, 438 (1993).
[29] F. Haider (private communication).